IEEE Access
Multidisciplinary | Rapid Review | Open Access Journal

Received February 11, 2019, accepted February 23, 2019, date of publication March 29, 2019, date of current version April 12, 2019.

Digital Object Identifier 10.1109/ACCESS.2019.2908289

Predictive Torque Control With Online Weighting Factor Computation Technique to Improve Performance of Induction Motor Drive in Low Speed Region

APEKSHIT BHOWATE, (Student Member, IEEE), MOHAN AWARE, (Senior Member, IEEE), AND SOHIT SHARMA, (Student Member, IEEE)

Electrical Engineering Department, Visvesvaraya National Institute of Technology, Nagpur 440010, India

Corresponding author: Apekshit Bhowate (apekshit.bhowate@students.vnit.ac.in)

ABSTRACT This paper presents a predictive torque control (PTC) method with online weighting factor computation based on the principle of coefficient of variation (CV) while maintaining the steady state, dynamic, and low-speed performance of three-phase induction motor (IM) drive. In PTC, appropriate weighting factor values are essential for the satisfactory performance of the drive. The main challenge is the tedious tuning of weighting factors, which requires rigorous simulation to obtain the desired performance of the drive. In this paper, a method is proposed that estimates online weighting factors, which modifies the cost function consecutively based on the principle of CV. In this method, the ranking of constraint is based on its magnitude of dispersion, whereas in other tuning methods, ranks are assigned beforehand. The proposed method (CV-PTC) is compared with the conventional normalized weighting factor-based PTC method specifically to improve the demagnetization effect in the low-speed operation. In the CV-PTC algorithm, synthetic voltage vectors are implemented to improve the performance of IM in full operating speed range. The experimental analysis is carried out on the IM drive prototype to validate the results and showcase the independence imparted for the selection of weights in the cost function.

INDEX TERMS Induction motor drive, predictive torque control, voltage source inverter, weighting factor.

I. INTRODUCTION

Adjustable speed drives and power converter control strategies have been in persistent advancements since the 1960's [1] having applications in all areas like defense, aerospace, marine, communication, mining, civil, transportation, medicine etc. Various control strategies like v/f control, space vector pulse width modulation (SVPWM), field oriented control (FOC), direct torque control (DTC) and model predictive control (MPC) have been used in variable speed drives for low, medium, and high power applications. FOC and DTC are the most widely used methods in industries for three phase variable frequency drives (VFD) [2]. DTC [3] is a lookup table based control approach in which a voltage vector is selected based on the stator flux angle and flux error, and torque error outputs of two hysteresis comparators. FOC gives less flux ripple, torque ripple, and current ripple than DTC, however, DTC gives a faster dynamic response ([4], [5]). A DTC technique is given in [6] with low torque ripple characteristics, constant switching frequency and reduced common-mode voltage (CMV). CMV in IM drives causes bearing leakage current, insulation breakdown of winding due to over voltage stress [7], and fault in current sensor circuit due to electromagnetic interference [8] which reduces the drive robustness.

MPC is considered a promising technology for medium power applications in VFD. MPC popularity is owing to its refined structure, easy inclusion of constraints in cost function and straightforward implementation. Recently finite set model predictive torque control (FS-PTC) approach for control of speed and torque of the motor by discretizing the motor dynamic equation was introduced. FS-PTC for an electrical drive with 2-level voltage source inverter is studied in experimentation for IM [9], [10], and permanent magnet

The associate editor coordinating the review of this manuscript and approving it for publication was Snehal Gawande.

synchronous motor (PMSM) [2], [11], [12] to achieve minimum torque ripple.

In PTC, switching frequency is confined by the sampling frequency. Ideally, the switching frequency is half of the sampling frequency but practically it is less than the former value which reflects in the form of high flux and torque ripples. Implementation of PTC using the graph algorithm is presented [13] in which switching frequency is reduced to 70% compared to linear control combined with PWM. A variable switching point PTC is discussed in [14], in which transition time of the state of switches is calculated along with good dynamic performance. In [15] a new switching strategy is proposed with MPC to obtain high efficiency and balanced loss distribution. A strategy is given in [16] presenting that switching losses of the converter can be reduced without affecting the output current quality.

With a 2-level inverter, in conventional PTC two zero voltage vectors and six active voltage vectors are used in every sampling period to optimize the performance of the electrical drive, initiating a prominent CMV due to zero voltage vector usage. In [17] three adjacent and one non-adjacent non-zero voltage vector is used in MPC to reduce CMV, switching frequency, and calculation burden. In [18], only two non-zero voltage vectors are selected from the optimized cost function with optimum time sharing that produce satisfactory stator current ripple with reduced CMV.

In PTC and all FS-PTC based controllers, there is absence of current PI controllers, the only parameter for tuning is the weighting factor in the cost function which decides the control objective. In [19] guidelines are given to empirically determining the weighting factor by classifying the cost function and weighting factor. An optimized weighting factor method is given in [9] to reduce the torque ripple by calculating torque ripple as a function of weighting factor. A PTC without weighting factor is discussed in [20] where the cost function is optimized based on the ranking approach this makes the tuning of weighting factor unnecessary for correct operation. The MPC discussed in [21] proposed a specialized sector distribution method to reduce the computation burden of the cost function. The PTC discussed in [22], torque and flux magnitude references are converted into an equivalent reference vector of stator flux hence eliminating the weighting factor. In the above discussed methods [9], [20]–[22] the cost function is modified such that weighting factors are eliminated so there is no need of tuning the weighting factors. A neural network based weighting factor estimation applied to predictive current controller (PCC) is given in [23]. A variable weighting factor based on current ripple is given in [24] where the weighting factor changes depending on the position and magnitude of the voltage vector. The weighting factors are calculated using Technique for Order of Preference by Similarity to Ideal Solution (TOPSIS), and VlseKriterijuska Optimizacija I Komoromisno Resenje (VIKOR) methods in [25], and [26] respectively. In the above two multi-criteria decision making (MCDM) methods both qualitative as well as quantitative parameters are considered but they cannot tackle problem of preference absence among the criteria. In these types of methods the preference to the criteria is given beforehand and remains fixed throughout the operation limiting the performance within the constraint.

This paper presents a MCDM method for tuning the weighting factor online by using coefficient-of-variation (CV) to tackle the problem of preference absence among the criteria. Here there is no necessity of giving preference to the criteria as the CV-PTC assigns the preference according to the amount of dispersion in the variables under control. Thus in every sampling the preferences are reassigned itself by the algorithm hence improvement in the complete operating speed range is feasible. A new cost function is constructed to target torque ripple and switching loss reduction with improvement in low speed operation. The constraints are analyzed and weights are assigned online for implementing the minimum cost function. The dynamic performance of the drive is retained while CMV reduction is observed. The stator flux drooping and destabilized torque control improvement in the low speed region operation with the use of synthetic voltage vectors is demonstrated experimentally in the proposed method.

The paper is arranged as, in Section II conventional PTC algorithm is discussed. Section III presents the cost function formulation for switching losses and CMV reduction. Section IV presents proposed PTC algorithm. Section V gives the experimental results followed by the conclusion.

II. CONVENTIONAL PTC FOR 2-LEVEL VOLTAGE SOURCE INVERTER

A. INDUCTION MOTOR MODELING

The stator and rotor equations describing IM model are given by (1) - (4).

$$v_s = R_s i_s + \frac{d\psi_s}{dt} \tag{1}$$

$$0 = R_r i_r + \frac{d\psi_r}{dt} - j\omega\psi_r \tag{2}$$

$$\psi_s = L_s i_s + L_m i_r \tag{3}$$

$$\psi_r = L_m i_s + L_r i_r \tag{4}$$

where,

v_s, and i_s are stator voltage and current.

i_r, rotor current.

R_s, and R_r are stator and rotor resistances.

L_s, L_r, and L_m are the stator, rotor and magnetizing inductances.

ψ_s, and ψ_r are the stator and rotor flux.

ω is rotor angular speed.

The electromagnetic torque T_e of the IM is given by (5).

$$T_e = \frac{3}{2} PIm\{\overline{\psi_s} i_s\} \tag{5}$$

T_e and P are electromagnetic torque and pole pairs.

$\overline{\psi_s}$ is the complex conjugate value of ψ_s.

For designing a controller, a mathematical model of the IM is derived with stator current i_s, rotor flux ψ_r, and rotor speed ω as state variables. Solving (1) - (5), stator and rotor

dynamics of squirrel cage IM are obtained in terms of stator current (6) and rotor flux (7) as;

$$i_s + \tau_\sigma \frac{di_s}{dt} = \frac{k_r}{R_\sigma}\left(\frac{1}{\tau_r} - j\omega\right)\psi_r + \frac{v_s}{R_\sigma} \tag{6}$$

$$\psi_r + \tau_r \frac{d\psi_r}{dt} = j\omega\tau_r\psi_r + L_m i_s \tag{7}$$

$$\frac{d\omega_m}{dt} = \frac{P}{J}(T_e - T_l) \tag{8}$$

where, $\omega = P\omega_m, k_r = \frac{L_m}{L_r}$, $\tau_r = \frac{L_r}{R_r}$, $\sigma = 1 - \frac{L_m^2}{L_s L_r}$, $R_\sigma = R_s + R_r k_r^2$, $\tau_\sigma = \frac{\sigma L_s}{R_\sigma}$, J denotes the moment of inertia of mechanical shaft, T_l is the load torque connected to the machine, ω_m is the mechanical rotor speed.

B. 2-LEVEL VOLTAGE SOURCE INVERTER

Fig. 1 shows a six switch (IGBT) voltage source inverter (VSI) connected to an IM. The two switches in each leg of VSI are operating complementary to each other thus producing eight possible switching states as given in Fig. 2. When the upper switch is 'ON' the VSI leg is clamped to +0.5 V_{dc} voltage and −0.5 V_{dc} when a lower switch is 'ON', for a dc link voltage of V_{dc}.

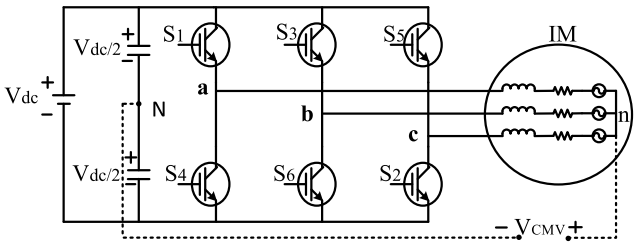

FIGURE 1. Topology of 2-level VSI.

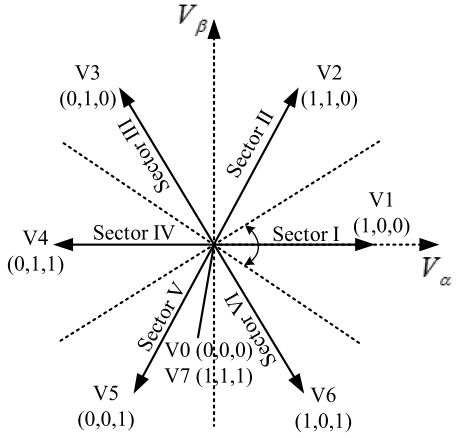

FIGURE 2. Switching states and voltage vectors of the 2-level VSI.

Thus the switching vector is defined as $\{S_x\} = [0, 1]\ \forall$ x = (a, b, c), where "0" represents inverter voltage when an only lower switch is 'ON' and "1" when an only upper switch is 'ON'.

The voltage vector which produces zero voltage are called as zero or null voltage vectors are [1 1 1] and [0 0 0]. The remaining six voltage vectors which produces a physical voltage at the output of inverter are called as active voltage vectors.

C. CMV IN THREE-PHASE INDUCTION MOTOR DRIVES

The potential between the ground of VSI and mid-point (N) of the DC bus capacitor is negligible. So CMV is measured between the star neutral-point (n) of IM and mid-point (N) of DC bus as shown in Fig. 1.

Mathematically CMV is calculated with reference to pole voltages as (9).

$$V_{cmv} = \frac{v_{aN} + v_{bN} + v_{cN}}{3} \tag{9}$$

where, V_{cmv} is the CMV of drive. v_{aN}, v_{bN}, and v_{cN} are the pole voltages of each phase.

Use of zero voltage vector leads to CMV of $\pm V_{dc}/2$ whereas that of active voltage vector gives $\pm V_{dc}/6$ [18]. Thus the use of only active voltage vector contributes to the reduction in CMV. But the use of only active voltage vector lead to distortion in stator current and increases the electromagnetic torque ripple.

D. MODEL PREDICTIVE TORQUE CONTROL

The stator flux, and rotor flux estimator are formulated using (1), (2), (3), and (4) using Euler's backward formula.

$$\overline{\psi_s}(k) = \overline{\psi_s}(k-1) + T_s v_s(k) + R_s T_s i_s(k-1) \tag{10}$$

$$\overline{\psi_r}(k) = \frac{L_r}{L_m}\overline{\psi_s}(k) + i_s(k)\left(L_m - \frac{L_r L_s}{L_m}\right) \tag{11}$$

By discretizing stator flux and stator current in (1) and (6) at $(k+1)^{th}$ time instant.

$$\psi_s^p(k+1) = \psi_s(k) + T_s v_s(k) - R_s T_s i_s(k) \tag{12}$$

$$i_s^p(k+1) = \left(1 + \frac{T_s}{t_\sigma}\right) i_s(k) + \left(\frac{T_s}{t_\sigma + T_s}\right) \times \left\{\frac{1}{R_\sigma}\left[\left(\frac{k_r}{t_r} - k_r j\omega\right)\overline{\psi_r}(k) + v_s(k)\right]\right\} \tag{13}$$

Now prediction of electromagnetic torque is done from (5), and the predicted value of stator flux (12), and stator current (13) as follows.

$$T_e^p(k+1) = \frac{3}{2} PIm\left\{\overline{\psi_s^p}(k+1) i_s^p(k+1)\right\} \tag{14}$$

The motor speed is estimated with a speed encoder and current, and dc bus voltage are sensed by using current and voltage sensors respectively. From the sensed values, the stator flux and the electromagnetic torque are predicted from (12) and (14) for all the values of voltage vector $v_s(k)$.

Finally inside the cost function the Euclidean distance of the predicted values from the reference values are evaluated for all the switching states. The cost function is composed of control law which governs the constraints on the variable

of the system. The voltage vector which gives the minimized values is chosen to be fired in the next control cycle. Fig. 3 shows the control structure of the conventional PTC scheme for 2-level VSI. Here the variables under consideration are electromagnetic torque and stator flux, so the structure of the cost function is given by (15).

$$g_h = \left|T_e^* - T_e^p\,(k+1)_h\right| + \lambda_\psi \left|\psi_s^* - \psi_s^p(k+1)_h\right| \quad (15)$$

where, weighting factor: $\lambda_\psi = T_n/\psi_{sn}$, $h \in [1, 2, \ldots, 7]$.

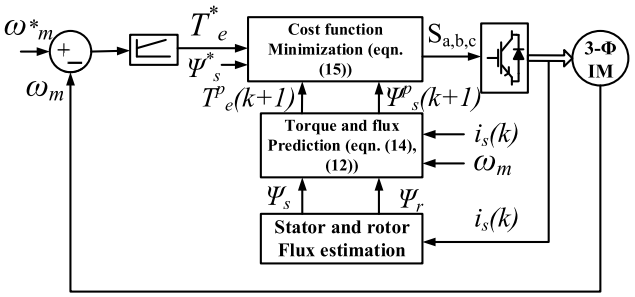

FIGURE 3. Control structure of PTC scheme for 2-level VSI.

The expressions in cost function are assigned weights to define the importance of the constraints which governs the system. In each cycle, evaluation of cost function for all voltage vectors is essential which increases the computational burden of the system. Annexation of more constraints like starting current and switching frequency in cost function further increases computation. The performance of the system is largely dependent on the weighting factor. But conventionally the weighting factor is estimated empirically so when the number of constraints increases, choosing weighting factor becomes challenging.

E. DELAY COMPENSATION

While implementing MPC in real-time hardware, one step time delay is introduced due to the calculation, which must be compensated. To solve this issue, prediction is done two steps ahead. The quantities obtained by calculation at $(k+1)^{th}$ time instant are used as initial values for prediction of $(k+2)^{th}$ values. So while calculating stator flux position instead of ψ_s, $\psi_s\,(k+1)$ is used. The cost function after implementation of delay compensation is given by (16).

$$g_h = \left|T_e^* - T_e^p\,(k+2)_h\right| + \lambda_\psi \left|\psi_s^* - \psi_s^p(k+2)_h\right| \quad (16)$$

where, weighting factor: $\lambda_\psi = T_n/\psi_{sn}$, $h \in [1, 2, \ldots, 7]$.

F. LOW SPEED DEMAGNETIZATION

The demagnetization of the stator flux occurs at the boundary of the sector [27]. To understand this, it is necessary to observe the flux maintaining capability of conventional voltage vectors (V_1-V_6). In Fig. 4, as the stator flux just enters the sector I, the voltage vector V_2 is selected and the stator resistance drop has major effect on the stator flux. The resultant stator flux produced is less when V_2 is applied for T_s time which causes demagnetization of stator flux as shown in Fig. 4.

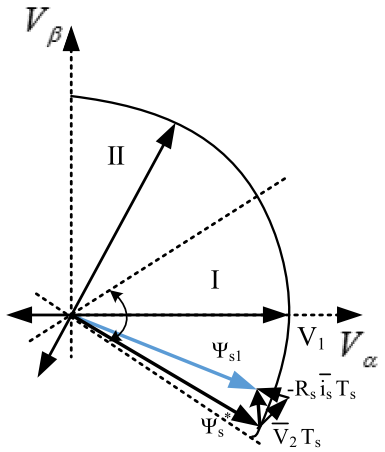

FIGURE 4. Effect of conventional voltage vector (V1-V6) at the sector boundary.

III. COST FUNCTION FORMULATION WITH SWITCHING LOSSES AND CMV REDUCTION

In the initial approach, switching losses of the system can be minimized by reducing the average switching frequency of the drive. The average switching frequency is calculated as (17).

$$f_{av} = \sum \frac{f_{sa} + f_{sb} + f_{sc}}{3} \quad (17)$$

To implement in hardware, the switching transitions are computed between the voltage vectors fired at previous sampling time and current sampling time. The switching transitions are given by (18).

$$C_{sw} = |S_a(k) - S_a(k-1)| + |S_b(k) - S_b(k-1)| + |S_c(k) - S_c(k-1)| \quad (18)$$

where C_{sw} gives the total number of switching in the converter in one sampling time. The cost function is constructed as (19).

$$g_h = \left|T_e^* - T_e^p\,(k+2)_h\right| + \lambda_\psi \left|\psi_s^* - \psi_s^p\,(k+2)_h\right| + AC_{sw} \quad (19)$$

where, $h \in [1, 2, \ldots, 7]$.

Due to the inclusion of the switching frequency, the cost evaluated will have a term containing the number of commutations and 'A' is the factor which gives weight to it. Thus by changing 'A' the average switching frequency of the drive can be changed. This is achieved by calculating the number of commutations in a sample time T_s.

Reducing the average switching frequency does not prominently minimize the switching losses, as it depends on the value of current and voltage across switch during commutation [28]. To accomplish the objective of increasing the efficiency of the drive, the switching losses are computed for every switching state and this constraint is added in the cost function, considering the assumption given in [29]–[32] that energy losses vary linearly with current and voltage at

commutation instant. During one commutation, energy loss in an IGBT switch is given by (20).

$$E_{loss} \propto K_1 \Delta i_c \Delta v_{ce} \tag{20}$$

where, K_1 is derived from the least-square approximation of measured data [33], i_c is the collector current, and v_{ce} is the collector-emitter voltage at the switching instant. Though this model does not consider all the complex aspects of switching, it gives a good approximation which can be computed in real-time and implemented in digital signal processor (DSP). The cost function is constructed including the efficiency constraint which penalizes power consumption so the switching states with higher energy losses are avoided. Also a constraint with CMV is introduced in cost function so the voltage vectors which reflects less CMV are selected. For a 2-level inverter the cost function is proposed in (21).

$$g_h = \left|T_e^* - T_e^p(k+2)\right| + \lambda_\psi \left|\psi_s^* - \psi_s^p(k+2)_h\right| + \lambda_{cmv}\left|V_{cmv}^* - \left|V_{cmv}^{k+1}\right|_h\right| + \lambda_{eff}\left|\Delta i_c \Delta v_{ce}\right|_h \tag{21}$$

where, $h \in [1, 2, \ldots, 7]$

λ_{eff} is the weighting factor which considers the importance of energy loss with respect to other quantities and Δi_c, and Δv_{ce} is the change in collector current and collector-emitter voltage of the IGBT switch. The collector current is the line current which is already being monitored and the collector-emitter voltage is the pole voltage of each phase which is calculated from the DC bus voltage which is being sensed. λ_{cmv} is the weighting factor of CMV of the drive.

IV. PROPOSED COEFFICIENT-OF-VARIATION PREDICTIVE TORQUE CONTROL (CV-PTC) FOR 2-LEVEL VSI

A. CONTROL STRUCTURE OF CV-PTC SCHEME

The complete block diagram and control strategy of the proposed CV-PTC scheme is shown in Fig. 5 and Fig. 6 respectively. A 2-level VSI is feeding a three-phase IM. The inverter DC bus is buildup by a three-phase uncontrolled rectifier. The speed loop is similar to that of DTC. Sensed currents, and voltage are given to the stator, and rotor flux estimators.

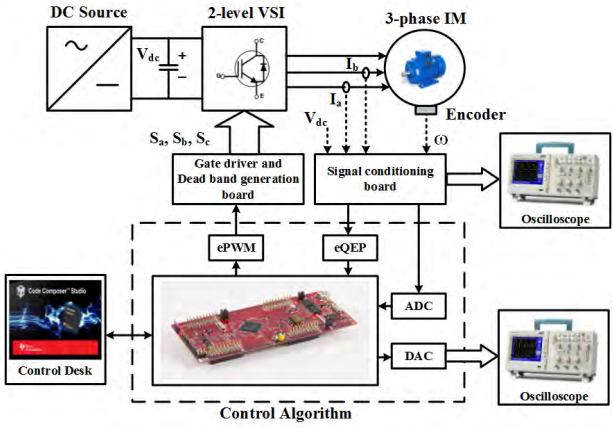

FIGURE 5. Block diagram of CV-PTC scheme for 2-level VSI.

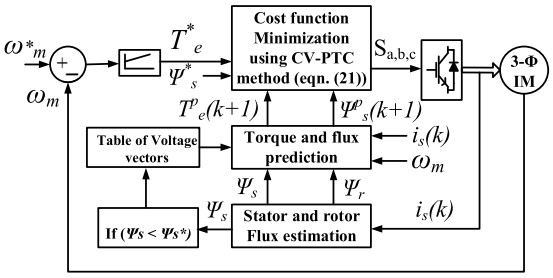

FIGURE 6. Control structure of CV-PTC scheme for 2-level VSI.

From the estimated values, torque, and flux predictions are done. The predicted values are compared with the reference values and used to select the appropriate switching state. The CV-PTC optimization method decides the weighting factor and assigns to the constraints in the cost function in every control cycle.

B. SELECTION OF VOLTAGE VECTORS AND OPTIMIZATION

CV-PTC is proposed for selecting a single switching state with respect to different constraints as discussed above and finding the optimal solution. A MCDM method proposed in [34] to tackle the problem of preference absence among the criteria is modified and adopted in CV-PTC for specifically considering torque, flux, CMV, and switching loss as control variables.

The CV-PTC algorithm steps are as follows;

Step 1: Generation of data-set

Step 2: Range standardization

Step 3: Compute the weights by coefficient-of-variation

Step 4: Rank the alternatives

For generation of data-set to apply proposed method, the cost function is disseminated into small singular cost functions of torque (22), flux (23), CMV (24), and switching losses (25) as given below.

$$E_T = \left|T_e^* - \left(T_e^{k+2}\right)_h\right| \tag{22}$$

$$E_\psi = \left|\left|\psi_s^*\right| - \left|\psi_s^{k+2}\right|_h\right| \tag{23}$$

$$E_{cmv} = \left|V_{cmv}^* - \left|V_{cmv}^{k+1}\right|_h\right| \tag{24}$$

where, $V_{cmv}^* = 0$

$$E_{eff} = \left|\Delta i_c \Delta v_{ce}\right|_h \tag{25}$$

where, E_T, E_ψ, E_{cmv}, and E_{eff} are cost functions for torque, flux, CMV, and switching losses respectively.

The flowchart of the CV-PTC algorithm is given in Fig. 7 and the steps are elaborated as follows:

Step 1 (Generation of Data-Set): Let various alternatives are denoted by x_{ij} where $i = 1, 2, \ldots m$ are number of switching states available and $j = 1, 2, \ldots n$ are number of control variables.

In this problem scenario the data-set will be of order 7×4 ($m \times n$). The selection of zero voltage vector (V_0 or V_7) for consideration in optimization is based on previous fired

active voltage vector. If (V_2, V_4 or V_6) is fired in previous control cycle then V_0 is selected else V_7 is selected. Thus there are seven switching vectors available. Control variables are torque, flux, CMV, and efficiency that is to be minimized. The sample data-set under consideration is given in Table 1. The sample data is collected from Texas instrument's code composer studio in real-time. The main objective of the cost function is to minimize the torque and flux ripple, reduce the CMV and switching losses, so the calculation of solution is done based on minimization.

TABLE 1. Dataset corresponding to switching vectors.

Switching Vector	E_T	E_ψ	E_{cmv}	E_{eff}
V_z	0.58	0.04	350	0.2
V_1	0.2	0.10	116.66	0.1
V_2	0.18	0.08	116.66	0.2
V_3	0.3	0.12	116.66	0.4
V_4	0.46	0.16	116.66	0.1
V_5	0.7	0.14	116.66	0.2
V_6	0.14	0.18	116.66	0.1

Step 2 (Range Standardization): This is done to convert all different units of criteria into common measurable units so as to compare the weights. The matrix obtained after range standardization is called as the normalized matrix. Range standardization is done as given by (26). The values obtained after evaluating the sample data-set is given in Table 2.

$$x'_{ij} = \frac{x_{ij} - \min\limits_{1\le j\le n} x_{ij}}{\min\limits_{1\le j\le n} x_{ij} - \min\limits_{1\le j\le n} x_{ij}} \tag{26}$$

Step 3 (Computation of Weights by Coefficient-of-Variation): Find the standard deviation independently for each criterion as given in (27).

$$\sigma_j = \sqrt{\frac{1}{m}\sum_{i=1}^{m}\left(x'_{ij} - \overline{x'_j}\right)^2} \tag{27}$$

$$\overline{x'_j} = \frac{x_{j1} + x_{j2} + x_{j3} + x_{j4} + x_{j5} + x_{j6} + x_{j7}}{7} \quad \forall j = 1, 2, 3 \ldots n \tag{28}$$

where, $\overline{x'_j}$ is mean of j^{th} control variable after being normalized and $j = 1, 2, 3, \ldots n$.

Now coefficient-of-variation for all the control variables is calculated as in (29).

$$CV_j = \frac{\sigma_j}{\overline{x'_j}} \tag{29}$$

The weights of the control variables can be evaluated as in (30).

$$w_j = \frac{CV_j}{\sum_{j=1}^{n} CV_j} \tag{30}$$

where, $j = 1, 2, 3, \ldots n$. The coefficient-of-variation and weights obtained after evaluating on sample dataset is given in Table 2.

TABLE 2. Range standardization of dataset and computation of weights by CV-PTC.

x'_{ij}	E_T	E_ψ	E_{cmv}	E_{eff}
V_z	0.786	0.000	1.000	0.333
V_1	0.093	0.429	0.000	0.000
V_2	0.071	0.286	0.000	0.333
V_3	0.286	0.571	0.000	1.000
V_4	0.571	0.857	0.000	0.000
V_5	1.000	0.714	0.000	0.333
V_6	0.000	1.000	0.000	0.000
$\overline{x'_j}$	0.401	0.551	0.143	0.286
σ_j	0.361	0.319	0.350	0.330
CV_j	0.901	0.579	2.449	1.155
$w_{j(CV-PTC)}$	0.177	0.114	0.428	0.227
$w_{j(PTC)}$	0.250	0.250	0.250	0.250

Step 4 (Rank the Alternatives): Apply the weights obtained in the designed cost function (31) for all the available switching states. The switching state with minimum cost is selected for firing the drive. The cost function values, and ranks after evaluation of sample data-set are given in Table 3.

$$g_h = \left[w_1 E_T + w_2 E_\psi + w_3 E_{cmv} + w_4 E_{eff}\right]_h \tag{31}$$

where, $h \in [1, 2, \ldots, 7]$ and w_1, w_2, w_3, w_4 are weights for torque, flux, CMV, and switching losses respectively.

For both PTC and CV-PTC cost function (31) is used to find the optimum voltage vector. The weights in PTC are normalized to 0.25 (as there are four criteria) and retained throughout the operation. The PTC method selects V_1 after optimization, which gives third highest torque ripple as given in Table 1. In the proposed CV-PTC method, the constraint with more dispersed values is given more importance [33] and assigned more weight and V_6 is selected as optimal voltage vector. This switching state gives lowest torque ripple as given in Table 1. The advantage of CV-PTC is the absence of preference assigned to control variables. So all the control variables are monitored simultaneously in every control cycle without giving any initial preference.

C. LOW SPEED PERFORMANCE

When PTC is implemented using the conventional voltage vectors then in low speed operation there is problem of drooping of flux and the poor torque control [1]. The drooping of flux occurs during the transition of stator flux

TABLE 3. Cost function ranking.

Switching Vector	PTC	CV-PTC	R_{PTC}	R_{CV-PTC}
V_z	87.705	68.800	7	7
V_1	29.267	56.285	1	6
V_2	29.282	56.302	6	5
V_3	29.372	56.373	4	3
V_4	29.347	56.338	3	4
V_5	29.427	56.401	2	2
V_6	29.272	56.284	5	1

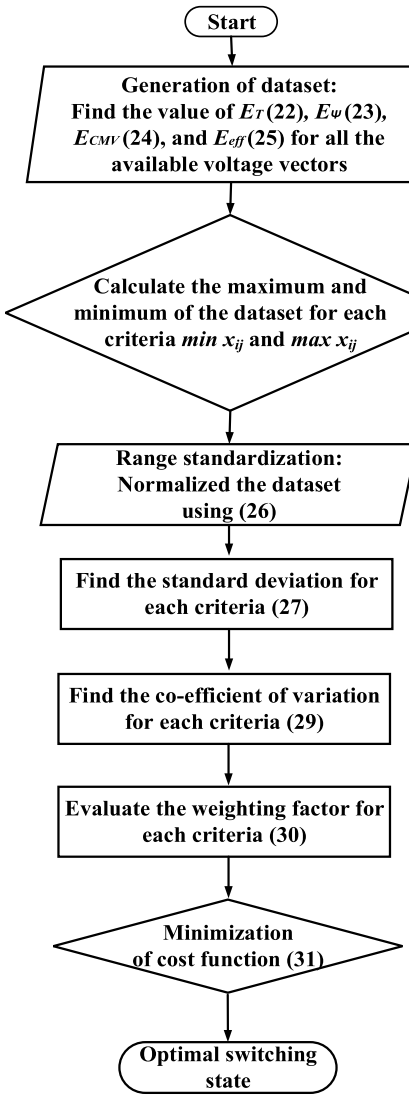

FIGURE 7. Flow chart of CV-PTC algorithm.

vector from k^{th} sector to $(k+1)^{th}$ sector. Also in low speed region, decrease of torque is difficult with zero voltage vector. In order to solve this problem, more number of voltage vectors are desirable. So six intermediate synthetic voltage vectors are generated using the existing active voltage vectors. The synthetic voltage vectors are shown in blue color in Fig. 8 and are numbered V_7 - V_{12}. The whole space is divided into 12 sectors of width 30^0 angular spread. There are total 12 voltage vectors which are now considered for minimization in cost function. The selection of voltage vectors is based on the rotor speed. When the rotor speed falls below 20% of rated speed of motor, then synthetic voltage vector along with conventional voltage vectors are considered for optimization.

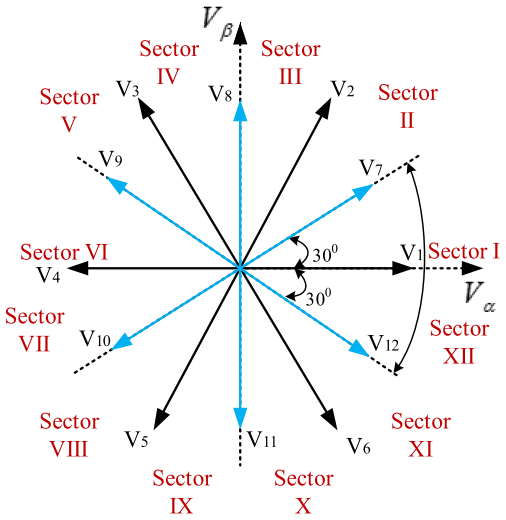

FIGURE 8. Subspace sector division for low speed operation.

To explain the stator flux generating ability of voltage vectors of both the strategies, consider the reference stator flux near the boundary of sector I and sector VI. In Fig. 9(a) it can be observed that the use of voltage vector V_2 causes the stator resistance drop to demagnetize the stator flux, thus the resultant stator flux decreases in PTC. The conventional voltage vectors are replaced by synthetic voltage vectors in CV-PTC and voltage vector V_7 is selected. The stator resistance drop in CV-PTC does not demagnetize so much as that in PTC as shown in Fig. 9(b). So even in low speed the flux is maintained in CV-PTC algorithm.

D. EXECUTION TIME ANALYSIS

The time taken for execution of CV-PTC algorithm is little more than PTC algorithm due additional step: Online computation of weights. The PTC algorithm requires less computation time since there is no need of calculation of weighting factor in it. However, the added online weighting factor calculations in CV-PTC algorithm are simple and time needed is less than the minimization and prediction time. The execution time graph comparison of both the algorithms are shown in Fig. 10. It can be observed that the execution time of PTC algorithm is 38.17μs. However, for CV-PTC algorithm the additional execution time for online weighting factor computation is 6.36μs. So the total execution time for CV-PTC algorithm is 44.62μs. It implies that the CV-PTC algorithm

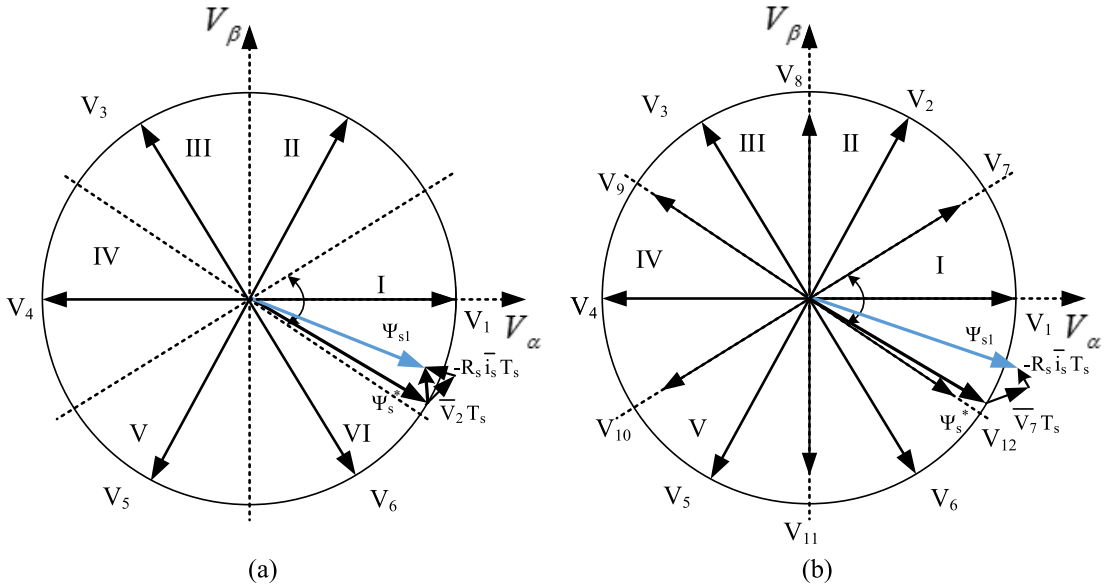

FIGURE 9. Diagram of stator flux generating capacity by voltage vectors for (a) PTC and (b) CV-PTC near the boundary of sector I.

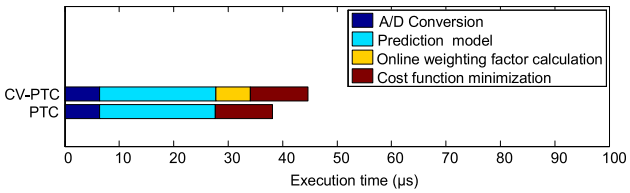

FIGURE 10. Execution time of PTC and CV-PTC algorithm.

can be implemented upto sampling frequency of 20 kHz which is sufficient for proper operation of the IM drive. The comparison of execution time required for different processes are shown in Table 4.

TABLE 4. Execution time of PTC and CV-PTC algorithm.

Execution time	PTC (μs)	CV-PTC(μs)
A/D conversion	6.36	6.37
Prediction model	21.30	21.33
Online weighting factor calculation	-	6.36
Cost function minimization	10.51	10.56
Total	38.17	44.62

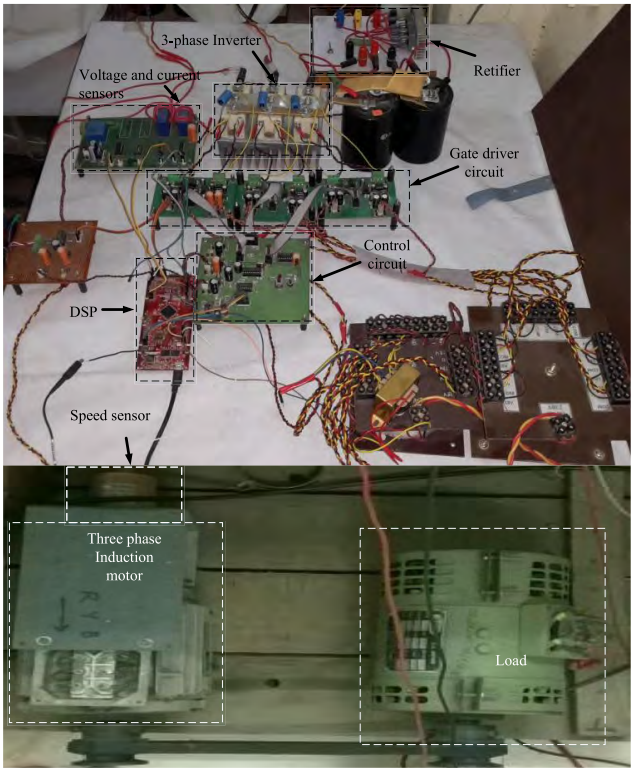

FIGURE 11. Experimental setup of induction motor drive.

V. EXPERIMENTAL RESULTS

The proposed algorithm has been verified experimentally in the laboratory. The experimental setup in Fig. 11 shows the squirrel cage IM coupled with the separately excited DC generator which is used as a load. The motor is driven by inverter, in which insulated gate bipolar transistor (IGBT) semiconductor switches are used along with gating drivers and control circuit which enables to give driving signals to the inverter. Texas instrument's TMS320F28377S digital signal processor is used for implementing the control algorithm. One voltage sensor (LV-25) is used to sense DC bus voltage and two current sensors (LA- 25P) are used to sense the current of two phases. The voltage and current are sensed

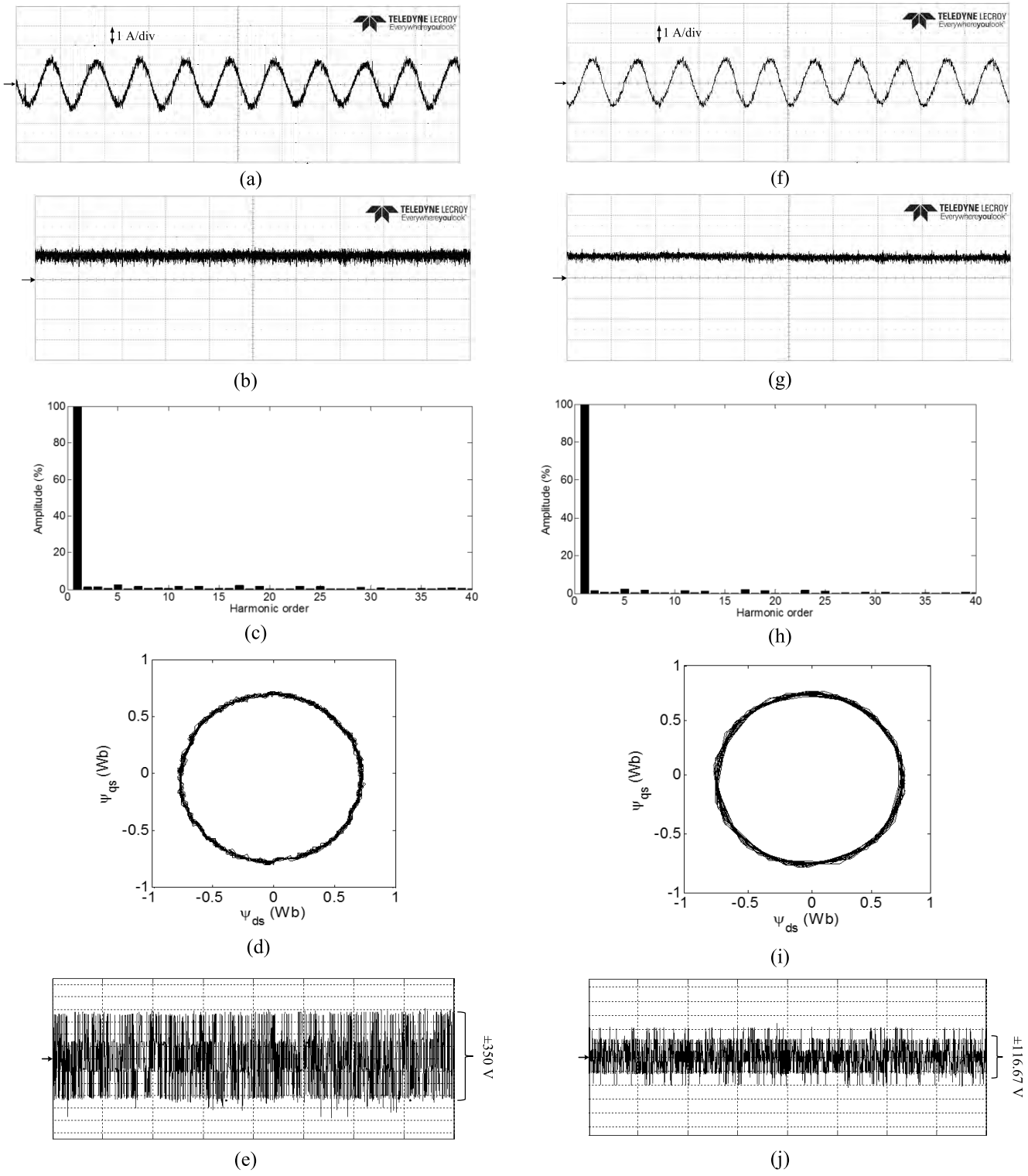

FIGURE 12. Experimental results during steady state at rated speed (1400 rpm) at 50% load. PTC: - (a) a-phase stator current [X-axis: 20 ms/div] (b) IM electromagnetic torque [X-axis: 10 ms/div, Y-axis: 2 Nm/div] (c) Stator current harmonic frequency spectra (THD = 3.42%) (d) Trajectory of dq stator flux (e) CMV of PTC [X-axis: 50 ms/div, Y-axis: 100 V/div]. CV-PTC: - (f) a-phase stator current [X-axis: 20 ms/div] (g) IM electromagnetic torque [X-axis: 10 ms/div, Y-axis: 2 Nm/div] (h) Stator current harmonic frequency spectra (THD = 3.26%) (i) Trajectory of dq stator flux (j) CMV of CV-PTC [X-axis: 50 ms/div, Y-axis: 100 V/div].

with a 12 bit on-board analog-to-digital converter (ADC) and the speed is sensed with a quadrature encoder pulse (QEP) with a resolution of 1500 pulse per revolution. The outputs of sensors are calibrated accordingly on the range of the ADC (0V - 3V) which is allowable on the DSP. The estimator and other variables are converted from digital-to-analog

values by on-board DAC so as to observe on a digital storage oscilloscope. The drive parameters for the IM used in the experimentation are given in Table 5.

TABLE 5. Parameters of the drive.

Parameter	Value
DC bus voltage, V_{dc}	700 V
Pole pairs, P	2
Rated power	0.75 kW
Inertia constant, J	0.047 Kg m^2
Rated flux, ψ_s	0.7 Wb
Stator resistance	1.2 Ω
Rotor resistance	1 Ω
Stator leakage inductance	175 mH
Rotor leakage inductance	175 mH
Mutual inductance	425 mH

A. STEADY STATE OPERATION

The cost function of CV-PTC is as inferred in (31). For every control cycle, the weighting factors are estimated online by the CV-PTC algorithm and are incorporated in the cost function. After inclusion of the weighting factors, the cost function is evaluated. To obtain a similar response in respect of rotor speed, for all the methods the same PI speed controller is applied. The performance of the drive is examined for both PTC and CV-PTC algorithms in the laboratory.

The flux reference is set at 0.7 Wb and the torque reference of 2 Nm is given. Fig. 12 shows the comparison of the PTC and CV-PTC schemes in steady state. Stator current for a-phase is shown in Fig. 12(a) and Fig. 12(f) for PTC and CV-PTC respectively. It can be observed that the torque ripple of PTC is 0.65 Nm (Fig. 12(b)) and CV-PTC is 0.45 Nm (Fig. 12(g)). The torque ripple was reduced by $\Delta T_e = 30\%$. CV-PTC (Fig. 12(c)) is having less THD (3.42%) than PTC (THD = 3.6%, Fig. 12(h)) due to the modified cost function and online tuning of weighting factors as discussed in Section III. The stator flux is plotted in the d-q plane for PTC and CV-PTC in Fig. 12(d) and Fig. 12(i) respectively which is same as given reference value of 0.7 Wb. Fig. 12(e) and Fig. 12(j) shows the CMV of PTC and CV-PTC respectively. The CMV of CV-PTC is reduced by 33.33% than that of PTC.

The steady state performance of CV-PTC is compared with PTC. The stator current THD plotted with respect to load in Fig. 13 which shows the reduction in THD for the proposed method. Electromagnetic torque ripple is plotted with respect to change in speed as given in Fig. 14 which shows a reduction of 30%. Fig. 15 shows a MATLAB surface plot comparing the phase current THD with different values of load current and sampling frequency. It can be observed that the CV-PTC method gives less THD than PTC method for various values of phase current and sampling frequency.

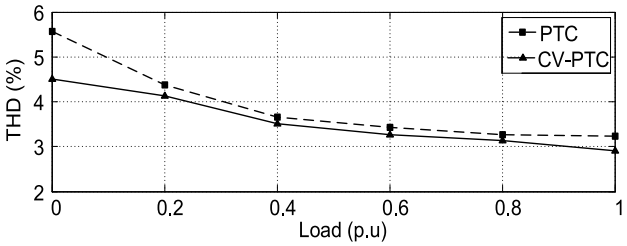

FIGURE 13. Experimental results: Variation of stator current THD at different load.

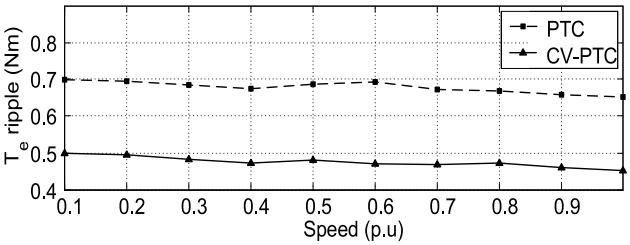

FIGURE 14. Experimental results: Variation of torque ripple at different speed.

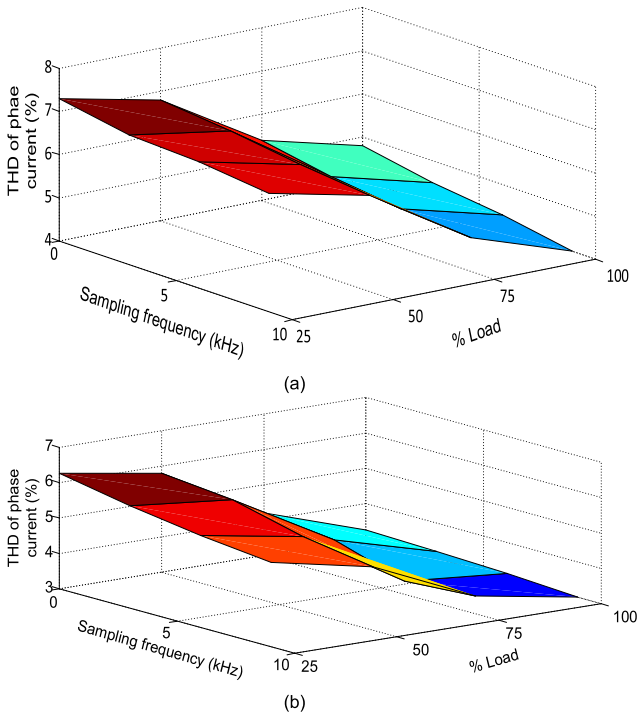

FIGURE 15. Surface plot for THD, sampling frequency and % load of (a) PTC and (b) CV-PTC algorithm.

B. LOAD TORQUE RESPONSE

For this test, the IM is maintained at a constant speed of 1000 rpm, and with the coupled DC motor a step load torque is given. Fig. 16 shows the torque maneuver of PTC and CV-PTC, as expected by the dynamics of the drive which is the same for both presented methods. The torque ripple for CV-PTC ($\Delta T_e = 0.45$ Nm) is less than that of PTC ($\Delta T_e = 0.65$ Nm). It is observed that the torque ripple for

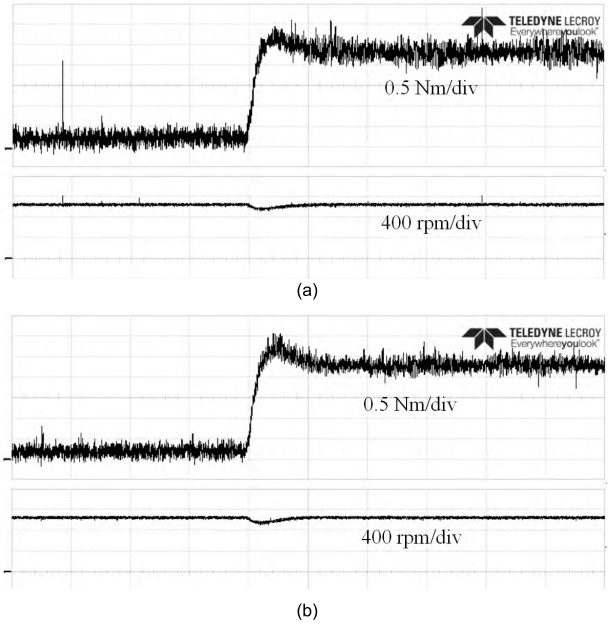

FIGURE 16. Step load torque change of (a) PTC and (b) CV-PTC [X- axis: 50 ms/div].

the proposed CV-PTC method is 29.85% lower than that of PTC.

C. SPEED REFERENCE STEP RESPONSE

Speed transients were tested by giving step speed change in the speed reference. The speed reference was changed when the IM is operating at no load. The rotor speed traces its reference value in 50 ms in both PTC (Fig. 17(a)) and CV-PTC (Fig. 17(b)). There are two loops designed: outer (speed) loop and inner loop; the later loop is faster than the previous. This gives freedom to increase the bandwidth of speed loop without interference [4]. It can be observed that the torque ripple in CV-PTC has reduced as compared to PTC.

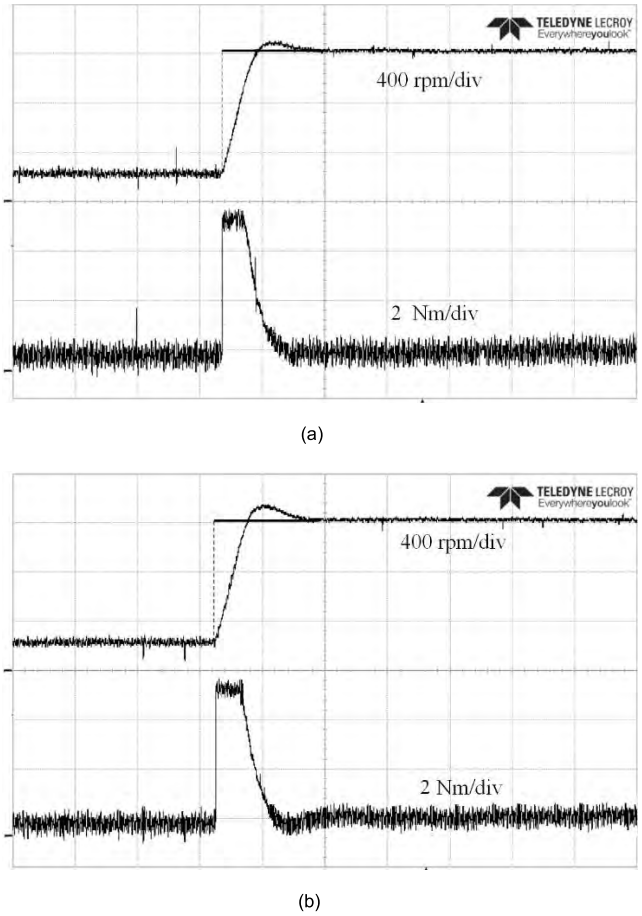

FIGURE 17. Step speed change of (a) PTC and (b) CV-PTC [X-axis: 50 ms/div].

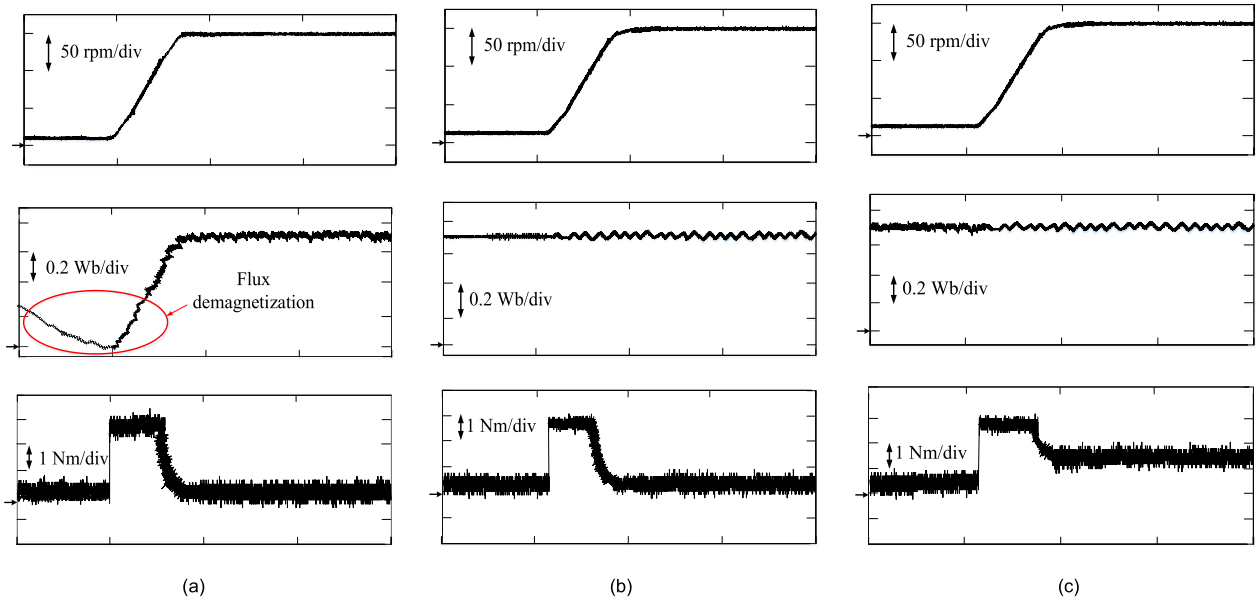

FIGURE 18. Experimental results under low speed operation [X-axis: 10 ms/div] (a) PTC with no load (b) CV-PTC with no load (c) CV-PTC with half load.

D. LOW SPEED OPERATION

The motor is given step speed reference with both the algorithm. Fig. 18(a) shows waveform of the drooping of flux during low speed operation of PTC algorithm. In PTC due to demagnetization effect the flux is deteriorated. Fig. 18(b) shows the experimental results with CV-PTC algorithm under low speed condition, the responses are comparatively remitted as compared with Fig. 18(a) and flux is maintained. Fig. 18(c) shows the low speed response under 1.5 Nm loaded condition. For CV-PTC algorithm the flux is maintained with some ripples also under loaded condition.

VI. CONCLUSION

In this paper, a modified cost function is formulated with four constraints i.e. torque, stator flux, CMV, and switching losses based on the CV-PTC optimization method, along with good, steady state as well as dynamic responses. In this method, the algorithm calculates the weighting factors online, which solves the problem of tuning. Also the necessity of giving of preference for control variables, which is essential in other online tuning methods, is eliminated in CV-PTC method. The essential importance of the constraints is considered by the CV-PTC optimization according to the steady state and transient behavior of the system. The presented method gives a good transient response in step speed change and step load torque change. In steady state operation, there is a 29.85%, and 33.33% reduction in torque ripple, and CMV respectively. Also the use of synthetic intermediate voltage vectors improves the low speed operation of the drive by maintaining flux. Furthermore, constraints like capacitor voltage balance, power factor etc. can be included in the cost function simply, with the proposed method. Also proposed method can be applied to other topologies like flying capacitor and three-level neutral-point clamped inverter.

REFERENCES

[1] S. Kouro, P. Cortés, R. Vargas, U. Ammann, and J. Rodriguez, "Model predictive control—A simple and powerful method to control power converters," *IEEE Trans. Ind. Electron.*, vol. 56, no. 6, pp. 1826–1838, Jun. 2009.

[2] M. H. Vafaie, B. M. Dehkordi, P. Moallem, and A. Kiyoumarsi, "A new predictive direct torque control method for improving both steady-state and transient-state operations of the PMSM," *IEEE Trans. Power Electron.*, vol. 31, no. 5, pp. 3738–3753, May 2016.

[3] J. W. Kang and S. K. Sul, "Analysis and prediction of inverter switching frequency in direct torque control of induction machine based on hysteresis bands and machine parameters," *IEEE Trans. Ind. Electron.*, vol. 48, no. 3, pp. 545–553, Jun. 2001.

[4] J. Rodriguez, R. M. Kennel, J. R. Espinoza, M. Trincado, C. A. Silva, and C. A. Rojas, "High-performance control strategies for electrical drives: An experimental assessment," *IEEE Trans. Ind. Electron.*, vol. 59, no. 2, pp. 812–820, Feb. 2012.

[5] A. Pal, S. Das, and A. K. Chattopadhyay, "An improved rotor flux space vector based MRAS for field-oriented control of induction motor drives," *IEEE Trans. Power Electron.*, vol. 33, no. 6, pp. 5131–5141, Jun. 2018. doi: 10.1109/TPEL.2017.2657648.

[6] J.-K. Kang and S.-K. Sul, "New direct torque control of induction motor for minimum torque ripple and constant switching frequency," *IEEE Trans. Ind. Appl.*, vol. 35, no. 5, pp. 1076–1082, Sep. 1999.

[7] S. Kwak and S. K. Mun, "Model predictive control methods to reduce common-mode voltage for three-phase voltage source inverters," *IEEE Trans. Power Electron.*, vol. 30, no. 9, pp. 5019–5035, Sep. 2015.

[8] M. J. Duran, J. A. Riveros, F. Barrero, H. Guzman, and J. Prieto, "Reduction of common-mode voltage in five-phase induction motor drives using predictive control techniques," *IEEE Trans. Ind. Appl.*, vol. 48, no. 6, pp. 2059–2067, Nov./Dec. 2012.

[9] S. A. Davari, D. A. Khaburi, and R. Kennel, "An improved FCS–MPC algorithm for an induction motor with an imposed optimized weighting factor," *IEEE Trans. Power Electron.*, vol. 27, no. 3, pp. 1540–1551, Mar. 2012.

[10] M. Habibullah, D. D.-C. Lu, D. Xiao, and M. F. Rahman, "A simplified finite-state predictive direct torque control for induction motor drive," *IEEE Trans. Ind. Electron.*, vol. 63, no. 6, pp. 3964–3975, Jun. 2016.

[11] Y. Wang *et al.*, "Deadbeat model-predictive torque control with discrete space-vector modulation for PMSM drives," *IEEE Trans. Ind. Electron.*, vol. 64, no. 5, pp. 3537–3547, May 2017.

[12] W. Xie, X. Wang, F. Wang, W. Xu, R. Kennel, and D. Gerling, "Dynamic loss minimization of finite control set-model predictive torque control for electric drive system," *IEEE Trans. Power Electron.*, vol. 31, no. 1, pp. 849–860, Jan. 2016.

[13] M. Preindl, E. Schaltz, and P. Thogersen, "Switching frequency reduction using model predictive direct current control for high-power voltage source inverters," *IEEE Trans. Ind. Electron.*, vol. 58, no. 7, pp. 2826–2835, Jul. 2011.

[14] P. Karamanakos, P. Stolze, R. M. Kennel, S. Manias, and H. du Toit Mouton, "Variable switching point predictive torque control of induction machines," *IEEE J. Emerg. Sel. Topics Power Electron.*, vol. 2, no. 2, pp. 285–295, Jun. 2014.

[15] S. Kwak and J.-C. Park, "Switching strategy based on model predictive control of VSI to obtain high efficiency and balanced loss distribution," *IEEE Trans. Power Electron.*, vol. 29, no. 9, pp. 4551–4567, Sep. 2014.

[16] O. Oñederra, I. Kortabarria, I. M. de Alegría, J. Andreu, and J. I. Gárate, "Three-phase VSI optimal switching loss reduction using variable switching frequency," *IEEE Trans. Power Electron.*, vol. 32, no. 8, pp. 6570–6576, Aug. 2017.

[17] L. Guo, X. Zhang, S. Yang, Z. Xie, and R. Cao, "A model predictive control-based common-mode voltage suppression strategy for voltage-source inverter," *IEEE Trans. Ind. Electron.*, vol. 63, no. 10, pp. 6115–6125, Oct. 2016.

[18] A. Bhowate and M. Aware, "CMV suppression using a new predictive direct torque control for induction motor," in *Proc. 7th India Int. Conf. Power Electron. (IICPE)*, Nov. 2016, pp. 1–6.

[19] P. Cortes *et al.*, "Guidelines for weighting factors design in model predictive control of power converters and drives," in *Proc. IEEE Int. Conf. Ind. Technol.*, Feb. 2009, pp. 1–7.

[20] C. A. Rojas, J. Rodriguez, F. Villarroel, J. R. Espinoza, C. A. Silva, and M. Trincado, "Predictive torque and flux control without weighting factors," *IEEE Trans. Ind. Electron.*, vol. 60, no. 2, pp. 681–690, Feb. 2013.

[21] C. Xia, T. Liu, T. Shi, and Z. Song, "A simplified finite-control-set model-predictive control for power converters," *IEEE Trans. Ind. Informat.*, vol. 10, no. 2, pp. 991–1002, May 2014.

[22] Y. Zhang and H. Yang, "Two-vector-based model predictive torque control without weighting factors for induction motor drives," *IEEE Trans. Power Electron.*, vol. 31, no. 2, pp. 1381–1390, Feb. 2015.

[23] O. Machado, P. Martín, F. J. Rodríguez, and E. J. Bueno, "A neural network-based dynamic cost function for the implementation of a predictive current controller," *IEEE Trans. Ind. Informat.*, vol. 13, no. 6, pp. 2946–2955, Dec. 2017.

[24] A. Abbaszadeh, D. A. Khaburi, H. Mahmoudi, and J. Rodríguez, "Simplified model predictive control with variable weighting factor for current ripple reduction," *IET Power Electron.*, vol. 10, no. 10, pp. 1165–1174, Aug. 2017.

[25] V. P. Muddineni, A. K. Bonala, and S. R. Sandepudi, "Enhanced weighting factor selection for predictive torque control of induction motor drive based on VIKOR method," *IET Electr. Power Appl.*, vol. 10, no. 9, pp. 877–888, 2016.

[26] V. P. Muddineni, S. R. Sandepudi, and A. K. Bonala, "Finite control set predictive torque control for induction motor drive with simplified weighting factor selection using TOPSIS method," *IET Electr. Power Appl.*, vol. 11, no. 5, pp. 749–760, 2017.

[27] Y. N. Tatte and M. V. Aware, "Direct torque control of induction motor with common-mode voltage elimination," *Electr. Power Compon. Syst.*, vol. 44, no. 20, pp. 2310–2324, 2016. doi: 10.1080/15325008.2016.1220998.

[28] S. Bernet, S. Ponnaluri, and R. Teichmann, "Design and loss comparison of matrix converters, and voltage-source converters for modern AC drives," *IEEE Trans. Ind. Electron.*, vol. 49, no. 2, pp. 304–314, Apr. 2002.

[29] A. D. Rajapakse, A. M. Gole, and P. L. Wilson, "Electromagnetic transients simulation models for accurate representation of switching losses and thermal performance in power electronic systems," *IEEE Trans. Power Del.*, vol. 20, no. 1, pp. 319–327, Jan. 2005.

[30] L. Helle, K. B. Larsen, A. H. Jorgensen, S. Munk-Nielsen, and F. Blaabjerg, "Evaluation of modulation schemes for three-phase to three-phase matrix converters," *IEEE Trans. Ind. Electron.*, vol. 51, no. 1, pp. 158–171, Feb. 2004.

[31] O. Al-Naseem, R. W. Erickson, and P. Carlin, "Prediction of switching loss variations by averaged switch modeling," in *Proc. 15th Annu. IEEE Appl. Power Electron. Conf. Expo. (APEC)*, New Orleans, LA, USA, vol. 1, Feb. 2000, pp. 242–248.

[32] M. Apap, J. C. Clare, P. W. Wheeler, and K. J. Bradley, "Analysis and comparison of ac-ac matrix converter control strategies," in *Proc. IEEE 34th Annu. Conf. Power Electron. Spec. (PESC)*, vol. 3, Jun. 2003, pp. 1287–1292.

[33] R. Vargas, U. Ammann, and J. Rodríguez, "Predictive approach to increase efficiency and reduce switching losses on matrix converters," *IEEE Trans. Power Electron.*, vol. 24, no. 4, pp. 894–902, Apr. 2009.

[34] M. F. El-Santawy and A. N. Ahmed, "CV-VIKOR: A new approach for allocating weights in multi-criteria decision making problems," *Life Sci. J.*, vol. 9, no. 4, pp. 5875–5877, 2012.

[35] K.-B. Lee, J.-H. Song, I. Choy, and J.-Y. Yoo, "Improvement of low-speed operation performance of DTC for three-level inverter-fed induction motors," *IEEE Trans. Ind. Electron.*, vol. 48, no. 5, pp. 1006–1014, Oct. 2001.

APEKSHIT BHOWATE was born in Sewagram, Wardha, India, in 1991. He received the Electrical Engineering (Electronics and Power) degree from Sant Gadge Amravati University, Amravati, India, in 2012, and the master's degree in power electronics and drives from the Vellore Institute of Technology, Chennai, India, in 2015. He is currently pursuing the Ph.D. degree from the Visvesvaraya National Institute of Technology, Nagpur, India. His Ph.D. study is focused on predictive control of multiphase phase induction motor drives. His research interests include model predictive control, induction motor drives, direct torque control, space vector control, and neutral-point clamped converter.

MOHAN AWARE received the B.E. degree in electrical engineering from the College of Engineering, Amravati, India, in 1980, the M.Tech. degree in power apparatus and system from IIT Bombay, India, in 1982, and the Ph.D. degree in direct torque control for induction motor drives from Nagpur University, Nagpur, India, in 2002.

From 1982 to 1989, he was a Design Officer at Crompton Greaves Ltd., Nasik, India. From 1989 to 1991, he was a Development Engineer with Nippon Denro Ispat Ltd., Nagpur. From 2001 to 2002, he was a Research Fellow with the Electrical Engineering Department, The Hong Kong Polytechnic University, Hong Kong. He is currently a Professor with the Department of Electrical Engineering, Visvesvaraya National Institute of Technology, Nagpur. He has authored or coauthored more than 200 technical papers in different journals and conference proceedings. His current research interests include multiphase electrical drives, distributed generation, energy storage systems, and power electronics.

Dr. Aware is a Commonwealth Academic Fellow.

SOHIT SHARMA received the B.Tech. degree in electrical engineering from the Government Engineering College, Ajmer, India, in 2012, and the M.Tech. degree in power systems from Jagannath University, Jaipur, India, in 2015. He is currently pursuing the Ph.D. degree with the Visvesvaraya National Institute of Technology, Nagpur, India. His current research interests include the grid-connected power converters and control of multiphase drive systems.